Journal of Materials Chemistry A

Accepted Manuscript

ROYAL SOCIETY OF CHEMISTRY

www.rsc.org/materialsA

Journal of Materials Chemistry A

ARTICLE

A novel Ni_3N/graphene nanocomposite as supercapacitor electrode material with high capacitance and energy density

Received 00th January 20xx,
Accepted 00th January 20xx

DOI: 10.1039/x0xx00000x

www.rsc.org/

Yu Yu,[a] Wenyu Gao,[a] Zongxu Shen,[a] Qing Zheng,[a] Hao Wu,[a] Xi Wang,[a] Weiguo Song,[b]* and Kejian Ding[a]*

A novel Ni_3N/Graphene nanocomposite of small Ni_3N nanoparticles anchoring on the reduced graphene oxide nanosheets has been successfully synthesized. Due to the quite small size of Ni_3N nanocrystals,the surface for faradic redox reaction of pseudocapacitive materials dramatically increases. The main issue of the volume change obstructing the pseudo-supercapacitor performance is concurrently resolved by the tight attachment of Ni_3N nanoparticles with flexible texture. Importantly, the two-step oxidation/reduction reaction between Ni(I) and Ni(III) endows this nanocomposite with large capacitance by providing more faradic charge. The kind of electrode material behaves excellently both in three-electrode and asymmetric supercapacitors. The biggest specific capacitance reaches to 2087.5 F g^{-1} (at 1 A g^{-1}), and its asymmetric supercapacitor cell with ethylene glycol modified RGO as negative electrode has a high energy density (50.5Wh kg^{-1} at 800 W kg^{-1}). The cell capacitance retentions exceed 80% after 5000 cycles at different high current densities, showing its promising prospectfor high-energy supercapacitors.

Introduction

Due to their outstanding advantages of high power performance, low maintenance cost, and long cycle life, supercapacitors are considered as a competitive and qualified candidate for energy storage. To keep abreast of the high energy density of Li ion battery, meticulous modifications on carbon materials and varieties of pseudocapacitive materials (i.e. oxides, hydroxides, conducting polymers) are being employed to fabricate supercapacitor devices with high specific capacitances and a high energy density for practical application.[1,2] Besides, the rate capability and reversibility are also under the most important consideration. Especially for the pseudocapacitors, their capacitances have been provided by the faradic redox reactions of active materials, and their poorness of electro-conductibility seriously obstructs the fast electron transport during the redox reactions, leading to extreme decline of capacitances at high rates. To overcome this, highly conductive and ductile carbonaceous materials (i.e. activated carbon, CNTs, graphene and mesoporous carbon) have been introduced to prepare carbon materials supporting composites.[3] Among these carbonaceous materials, graphene, mainly including reduced graphene oxide (RGO), should be the most suitable option to load the nanoscale pseudocapacitive materials, owing to its two-dimensional structure with considerable high electrical conductivity, flexibility, mechanical strength and large specific surface area, as well as light weight.[4]

Nickel compounds are one kind of the most studied pseudocapacitive materials, with their advantages of inexpensive cost, high theoretical capacity and pseudocapacitive reaction reversibility.[5] Various nanostructures of nickel oxide and hydroxide (nanoparticles,[6] nanowire,[7] nanosheets,[8] assemblages,[9] etc), and their composites with conductive carbonaceous materials (CNTs,[10] graphene,[11,12] etc) were studied, and all showed comparatively well performance. However, the faradic redox reaction during +2 and +3 valent Ni only provides a certain quantity of electric charge. In general, Ni elements are bound to be oxidized to +3 valent in the frequently-used alkaline electrolyte and voltage range. Therefore, if Ni elements in pseudocapacitors are equipped with the lower reduced state (i.e. +1 and 0) with the nearby redox potential, nickel species will bring out more faradic charge during the reaction between the low valent and +3 Ni, further resulting in massive increase of specific capacitance.

Transition metal (especially IIIV group) nitrides could be composed in various and high metal/nitrogen proportions, with the low plus valent of metal atoms. Being subjected to the high resistivity, high hardness, great lattice and volume change arising from the corresponding reaction, most of metal nitrides (except TiN, MnN and VN)[13] behave disappointingly in supercapacitors.[14] For nickel nitride, it was widely researched as anode materials Lithium[15] and Sodium[16] batteries, but rarely for application in supercapacitors.

[a] School of Sciences, Beijing Jiaotong University, Beijing, 100044, P. R. China. Email: dkjian@bjtu.edu.cn
[b] Institute of chemistry, Chinese academy of sciences, Beijing, 100190, P. R. China. Email: wsong@iccas.ac.cn

†Electronic Supplementary Information (ESI) available: more SEM, TEM, XPS, and EDS results of Ni_3N/RGO, Ni_3N nanoparticles, and nickel hydroxide hydrate/RGO precursor, C and O XPS spectra, more ragone plots. See DOI: 10.1039/x0xx00000x

Herein, we reported a kind of graphene based composite, in detail, small Ni_3N nanoparticles anchoring on the reduced graphene oxide nanosheets (denoted as Ni_3N/RGO). The electro-conductibility and volume change of Ni_3N was extremely improved by the highly electro-conductive RGO matrix and nanocrystallization. On such composite electrode material, the specific capacitance up to 2087.5 F g^{-1} was achieved at 1 A g^{-1} in the three-electrode system in alkaline electrolyte. This kind of nanocomposites was also be fabricated to the asymmetric supercapacitors, with diethylene glycol grafted RGO (denoted as DEG/RGO) as negative electrodes. The energy density of device could be up to 50.5 Wh kg^{-1} at the average power density of 800.0 W kg^{-1}, and the device capacitances were maintained above 80% after 5000 cycles at high current density.

Experimental

Preparation of the Ni_3N/RGO Nanocomposite

All of the chemicals were directly used without further purification. Firstly, the graphene oxide (GO) was prepared according to the modified Hummer's method.[17] The Ni_3N/RGO nanocomposite was obtained by a solvothermal treatment and following annealing under ammonia atmosphere. Typically, a 6 mL portion of 3 mg/mL GO aqueous or alcoholic mucus was added into 44 mL glycol to form a uniform 0.3 mg/mL brown-colored suspension by vigorous stirring and ultrasonication. A 10 mL glycol solution dissolving 3.5 mmol $Ni(NO_3)_2{\cdot}6H_2O$ and a portion of 2 mL $NH_3{\cdot}H_2O$ (28 wt%) were then sequentially dropwise added into the suspension under stirring. After 10 min, the suspension was sealed in a 100 mL Teflon-lined stainless steel autoclave to perform solvothermal process at 150 °C for 10 h. After completion of the solvothermal reaction, the product was washed using absolute ethanol and deionized water several times to remove remnant glycol solvent molecules and inorganic salts ingredient, then dried in a freezer dryer. The clean and dried sample was then annealed for 2 h at 350 °C under NH_3 flow. The flow velocity of NH_3 flow and rate of temperature rise were 20 sccm and 5 °C min^{-1}.

Characterization

SEM images accompanied with EDS results and TEM images were taken on scanning electron microscopy (JEOL-6701F) and transmission electron microscopy (JEOL-2100F) respectively. X-ray diffraction (XRD) patterns were recorded on a Rigaku diffractometer (Maxima XRD-7000) using Cu Ka irradiation. TGA analysis was conducted on a Pyris 1 TGA Differential scanning calorimeter under air atmosphere at heating rate of 10 °C/min. Raman spectra and XPS information were obtained on Nicolet iN10 MX FT-IR Microscope, Thermo Scientific Raman microscope and ESCALab220i-XL photoelectron spectroscopy respectively. The specific surface area and pore size distribution were measured by BET on an Autosorb-1 analyzer.

Electrochemical Measurements

For preparing the electrodes of Ni_3N/RGO, the nanocomposite was mixed with poly(tetrafluoroethylene) binder with the mass ratio of 90:10 in a certain amount of ethanol to form a uniform slurry. The slurry was coated on the nickel foam current collector, which was then subjected to a 2 h drying in the atmosphere, followed by a tabletting at 4 MPa and 24 h drying at 80 °C in vacuum to remove ethanol and moisture thoroughly. The masses of active components coated on each nickel foam current collector were in the range of 2 - 3 mg. Electrochemical measurements were carried on an electrochemistry workstation (CHI660E, CH Instruments) in 6 M KOH within a three-electrode system, where a Pt sheet and Ag/AgCl (in saturated KCl) were employed as counter and reference electrodes respectively. EIS measurements were conducted on Princeton PARSTAT 2273 in the frequency range of 0.1 – 100 kHz.

Supercapacitor Devices

DEG/RGO was first prepared according to our previous work.[18] The fabrication of negative electrodes was similar to Ni_3N/RGO positive electrodes. In order to obtain good electrochemical performance for asymmetric supercapacitor, the mass ratio of positive to negative electrodes and voltage window were optimized to be around 0.34 and 1.6 V, while the electrolyte was also 6 M KOH. The masses of active components on positive and negative electrodes were about 3 and 10 mg respectively, and the areas of active components were about 4 cm^{-2}. The capacitance of asymmetric supercapacitor was calculated from galvanostatic charge-discharge curves as follows: $C = It/(Um)$, where m was the total mass of active materials both in the two electrodes, and I, t, and U were the discharge current, discharge time, and potential change. The energy and power density were elicited as: $E = CU^2/2$ and $P = E/t$.

Results and Discussion

Fabrication of the Ni_3N/RGO Nanocomposite

The Ni_3N/RGO composites were synthesized via a solvothermal method using ethylene glycol as solvent, followed by annealing under NH_3 at 350 °C, to convert the nickel hydroxide hydrate precursor into Ni_3N phase, as Fig. 1a presented. The XRD patterns (Fig. 1c) demonstrated the hexagonal nickel nitride phase (PDF#89-5144) of the annealed composites, and no signals corresponding to NiO, $Ni(OH)_2$ or other oxyhydroxide were detected. Meanwhile, no peaks subjected to RGO appeared, due to their fewer layers, poor crystalline and weak diffraction characteristics compared to Ni_3N phase. However, as the SEM image (Fig. S1a and b) showed, the graphene oxide sheets were corrugated into a curly and wavy shape, as most previous work involving the annealed GO reported. Homogeneously and uniformly distributed Ni_3N nanoparticles in the size of about 10 nm (Fig. 1b) were visibly attached to the surface of RGO. The consistent elucidation was also exhibited in TEM images (Fig. 1d). No other detached nanostructures could be found in the composition, even after vigorous

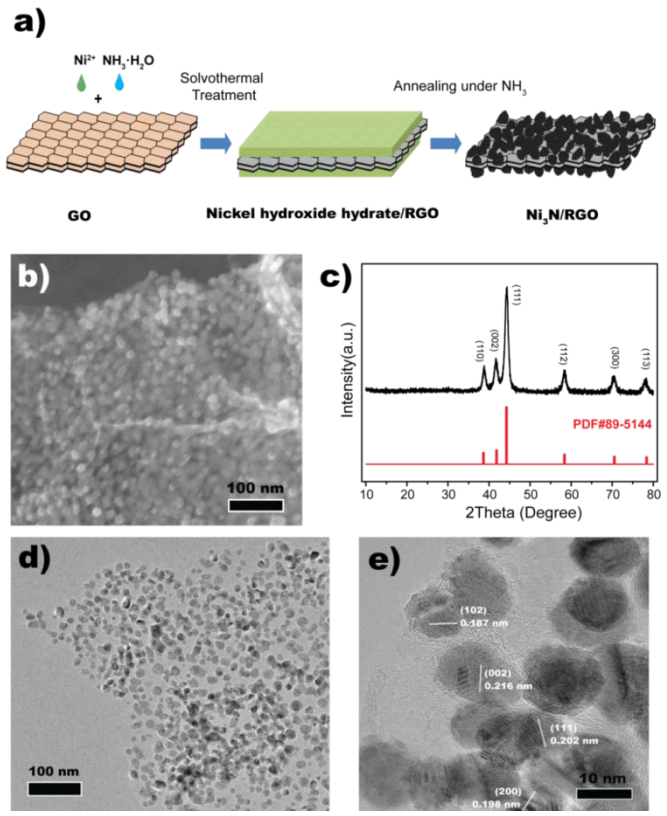

Fig. 1 (a) Synthesis scheme, (b) SEM image, (c) XRD pattern, (d) TEM, and (e) HRTEM images of Ni_3N/RGO nanocomposite.

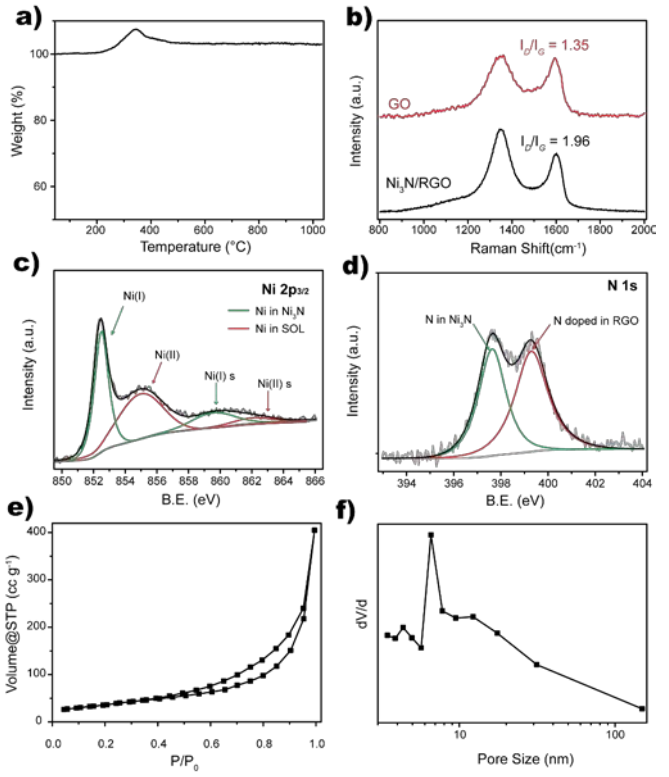

Fig. 2 (a) TGA result, (c) Ni $2p_{3/2}$ and (d) N 1s XPS spectra, (e) N_2 adsorption-desorption isotherm curve, and (f) pore distribution of Ni_3N/RGO nanocomposite; (b) Raman spectra of GO (above) and Ni_3N/RGO (below).

ultrasonic treatment during the sample preparing process, indicating the strong conglutination of Ni_3N particles onto the RGO flakes. Dense distribution and uniform dispersion of Ni_3N particles signified the heavy loading on the conductive texture, further bringing in high utilization of the electrochemical active component and high capacitance. In the high resolution TEM image (Fig. 1e), uniform fringe spaces of 0.216, 0.202, 0.198 and 0.187 nm, indexed to (002), (111), (200) and (111) lattices of the hexagonal Ni_3N respectively,[15,19] emerged from several of these small particles, confirming the results from phase analysis by XRD. EDS information (Fig. S1d) also indicated that Ni, C, and N were the main elements in the composite, while little O element existed, which would be discussed later.

In contrast to the nucleation and crystallization of nickel component in the aqueous condition of hydrothermal process, that in the alcohol phase of this solvothermal treatment was much moderate and slow.[20] So, it showed a lower crystallization degree. With the presence of graphene flakes, nickel hydroxide hydrate was formed as a weakly crystallized thin coating on the graphene sheets, for no obvious crystalline grains were observed from SEM and TEM images of the precursor (Fig. S2 a - d). It offered the hotbed of the dense distribution of small Ni_3N nanoparticles after the annealing under NH_3.

The loading mount of Ni_3N was measured by TG analysis. Firstly, pure Ni_3N was heated to 1000 °C in air to investigate the weight change. After completely converting to oxide, the single compound displayed a weight increase of about 17.1 % (Fig. S3), which was very close to the theoretical value. For Ni_3N/RGO, the weight increase occurred at 250 °C as shown in Fig. 2a, much earlier than pure Ni_3N due to their higher combustion activity of smaller nanoparticles. After 350 °C, an obvious weight loss happened, which was mainly attributed to the burning of RGO. The remaining weight was about 2.1 % higher than initial, and it could be estimated that the weight ratio of Ni_3N in composites was about 86.4 %.

The Raman spectra of GO and Ni_3N/RGO composite were shown in Fig. 2b. For GO, the intensities ratio of two prominent bands around 1340 and 1580 cm^{-1} assigned to the D and G bands in GO was 1.35, demonstrating a deeply oxidized state of GO. An apparent increasing of I_D/I_G was observed on Ni_3N/RGO, which was a common phenomenon in chemical reduction of exfoliated graphite oxide.[21,22] The introduction of the defect including doping of N greatly contributed to the enhancement of D band,[23] while the conjunction of Ni_3N nanoparticles with the graphene was another significant cause of the decrease in the average size of the sp^2 domains.

The valence states of main elements in Ni_3N/RGO were studied by XPS. As the Ni $2p_{2/3}$ spectrum by peak fitting in Fig. 2c showed, the strong peak at 852.4 eV represented for +1 Ni element in Ni_3N phase,[24,25] and the weak peak at 859.5 eV was its satellite peak. Besides, the peak at 855.0 eV and its satellite peak at 862.1 eV ascribing to +2 Ni indicated the little presence of the higher positive valence Ni.[26] It was reported that the

transition metal nitride was of a certain extent of instability in moist air, to be partially oxidized to oxynitride.[27] Considering the nanometer effect caused by the small size of Ni_3N nanoparticles in Ni_3N/RGO, and combining the fact of the absence of other phase by XRD characterization, it is reasonable to infer that there was little NiN_xO_y composition in the thin layers of outside surface of Ni_3N. It is worth noting that N elements also could be divided to two types (Fig. 2d), of which the signal at 397.4 eV derived from -3 N in Ni_3N,[24,25] while another set at 399.3 eV was from the high valence N doped in RGO.[23] An accordant observation exhibited in C 1s spectrum of Fig. S4a, excepting from the strict aromatic C, some N bonding sp^2 and sp^3 C were seen.[23,28,29] The signal from hydroxy-bongding and carboxyl C at about 287 eV[18] extremely decread, indicating the recution of RGO in the solvothermal and annealing process, which was agreed with Raman spectra. In our previous work,[18] it was found that polyalcohol was greatly likely to graft onto the surfaces of RGO during the solvothermal process. Similar incidents occurred in this experimental system, as a result, some O bonding C was also detected in the composites.[18,29] It was well agreed with by O 1s spectrum (Fig. S4b), in which O 1s peak was resolved into ones indexed to oxynitride O in NiN_xO_y and ether O grafted in RGO.[30] For the aqueous electrolyte supercapacitors, both the doping of N and retaining of hydroxyls/carboxyls on the RGO could endow Ni_3N/RGO composites with favorable hydrophilicity and good wettability with electrolyte.

Electrochemical Performance of the Ni_3N/RGO Electrode

To investigate the application of the Ni_3N/RGO nanocomposites on supercapacitors, the dried and clean samples were deposited onto a Ni foam supporter and compressed into very thin chips as the supercapacitor electrodes in a three-electrodebeaker cell with a Ag/AgCl (in saturated NaCl) reference electrode. Cyclic voltammogram(CV) measurements were carried out in 6 M KOH aqueous alkaline solution electrolyte. Fig. 3a showed the cyclicvoltammetry (CV) curve of the Ni_3N/RGO composite at 20 mV s^{-1}. Dramatically different from the Ni(II) and Ni(III) nickel compounds reported before,[8-12] i.e. NiO, $Ni(OH)_2$,NiOOH, a wide and amalgamative pair of redox peaks was observed. By peak splitting, this pair of redox peaks could be regarded to consist of two pairs. The set of anodic peak at 0.37 V and cathodic peak at 0.12 V were attributable to the well-known reversible reactions of Ni(II) → Ni(III). For Ni_3N, Ni elements were of +1 valence, which was confirmed by the previous extensive study and XPS survey here. Thereupon, in the process of anodization of Ni_3N, Ni(I) elements were oxidized into Ni(II) state, then further to Ni(III). Similarly, Ni(II) component reduced from Ni(III) were sequentially reduced into Ni(I). As the same as the reactions of Ni(II) → Ni(III), the conversion between Ni(I) and Ni(II) was also reversible, giving a pair of redox peaks at 0.32 V and 0.07 V respectively. This novel and distinctive redox mechanism was expected to producemuch more faradic reaction pseudo-capacitance in the charge-discharge cycle. The Ni $2p_{3/2}$ XPS spectrum of positively charged Ni_3N/RGO in Fig. 3b

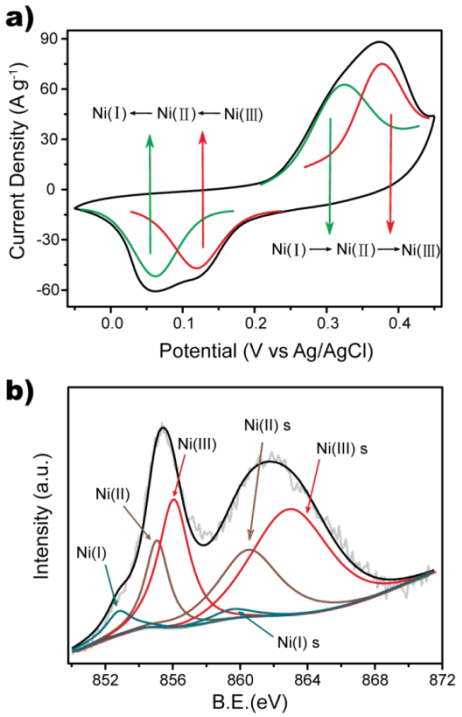

Fig. 3 (a) CV curve of Ni_3N/RGO electrode at scan rate of 20 mV s^{-1}, with a Pt sheet and Ag/AgCl (in saturated KCl) as counter and reference electrodes respectively, in 6 M KOH. (b) Ni $2p_{3/2}$ XPS spectrum of Ni_3N/RGO electrode materials after positive charging.

demonstrated the formation of Ni(III) component (856.4 eV) after charging, while some Ni(II) component produced by incomplete faradic reaction and mere unreacted Ni(I) component in the internal region of the nanoparticles were also detected.

CV testings at different scanning rates varying from 5 and 100 mV s^{-1} were done. As shown in Fig. 4a, all the CV curves exhibited the analogous current characteristics of two-step redox reaction. The average specific capacitance (C_s) of the Ni_3N/RGO composites was calculated to be 1580.2 F g^{-1} (based on total active mass, including RGO) at the scanning rate of 5 mV s^{-1}. The C_s against the scanning rate calculated by CV curves displayed in Fig. 4c. As the scanning rate increased from 5 to 100 mV s^{-1}, C_s could still maintain considerable high values above 750 F g^{-1}, which offered this kind of nanocomposites moreprospects for the practical application at high power densities.

The capacitances of Ni_3N/RGO were also measured by the galvanostatic charge/discharge. The discharge curves at the current densities in range of 5 - 100 A g^{-1} were showed in Fig. 4b (the discharge curves at 1 and 2 A g^{-1} not showed here). The charge/discharge current densities were applied in quite large region, which was more meaningful and instructive for practical application. Although it was hard to distinguish the two stages corresponding to the two step of cathodic reaction, all the curves displayed a discharging platform at 0.1 - 0.2 V. The biggest calculated specific capacitance was 2087.5 F g^{-1}at

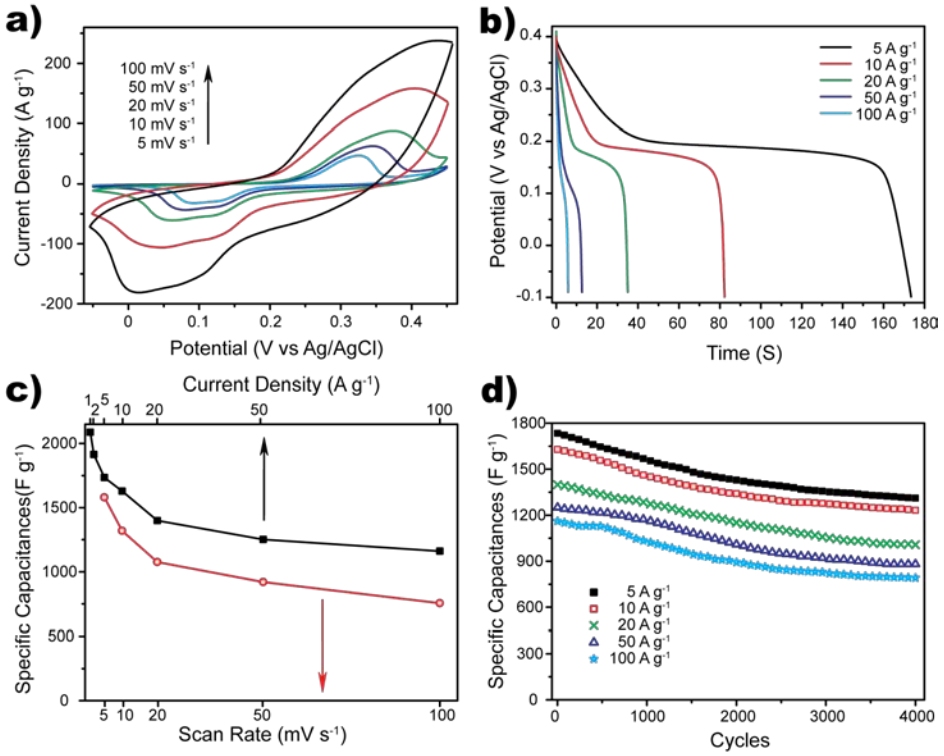

Fig. 4 (a) CV curves at various scan rates of 5 - 100 mV s^{-1}, (b) galvanostatic charge/discharge voltage profiles at various current densities of 5 - 100 Ag^{-1}, (c) the specific capacitances calculated by CV curves and galvanostatic charge/discharge voltage profiles, and (d) cycling stability at the different applied current densities of Ni_3N/RGO electrodes.

the lowest current density of 1 A g^{-1}. As the current densities enlarged, C_s dropped as expected, but not by a big extent. The specific capacitances at 2, 5, 10, 20, and 50 A g^{-1} acquired from Fig. 4c were 1913.8, 1734.7, 1629.0, 1398.8, and 1251.3 F g^{-1} respectively. Even at a high current density as 100 A g^{-1}, the specific capacitance was measured as high as 1160.8 F g^{-1}, about 56% of that at 1 A g^{-1}. The relatively high retention of C_s at high current density signified that the Ni_3N/RGO was of good rateperformance and power capability.

Many studies had shown that varieties of graphene and RGO derivatives could be gifted with electrochemical double-layer capacitors performance by the reasonable modification.[31,32] Also in our previous work about diethylene-glycol modified RGO, the graphene based materials analogous to the RGO in this work were measured to possess the double-layer capacitances at about 200 F g^{-1}.[18] However, the weight fraction of RGO in Ni_3N/RGO composites was only about 13.6 %, and the surface of graphene flake was mostly occupied by Ni_3N nanoparticles. Consequentially, the vast majority of specific capacitance of Ni_3N/RGO was contributed by Ni_3N component, and the RGO texture played an important role as flexibleconductive substrates. For comparison, the specific capacitance of pure Ni_3N synthesized by the same procedure as Ni_3N/RGO except from the adding of GO was measured. As Fig. S5 revealed, in contrast to Ni_3N/RGO, pure Ni_3N demonstrated extremely poor pseudo-capacitance performance. C_s values of pure Ni_3N were no more than 100 F g^{-1} at the current densities from 1 - 20 A g^{-1}. The result agreed well with others' studies on the supercapacitors application of transition metal nitrides, most of which performed badly with only a few tens F g^{-1} except VN, TiN and MnN.[14] It was worth noting that, contrary to the frequently reported nitrides, Ni_3N exhibited the pseudo-capacitance in the more positive voltage range, which was similar to other nickel compounds.

The important reason for the significant improvement on the capacitance of Ni_3N/RGO was that the size of Ni_3N was quite smaller, at about 10 nm, than that of pure Ni_3N (in the range of 50 - 200 nm, in Fig. S6a and b). As well known, the quasi-reversible redox processes always occurred on the surface or near surface of the active compounds particles.[1] The smaller size of Ni_3N nanoparticles produced more surfaces for the faradic reaction. As mentioned above, in the N_2 adsorption isotherms, the specific surface area of Ni_3N/RGO composites was measured to be about 132.8 m^2g^{-1}, almost 6 times that of pure Ni_3N (23.3 m^2 g^{-1}). What the crystal miniaturization brought was not only the increase of faradic surface, but also the mitigation of restriction by volume change during the redox reaction. Volume change was one of the most impactive factors for pseudocapacitive materials,[33] the structural breakdown from which also could be improved by Ni_3N nanoparticles' tight attachment with flexible texture.[34] The high hardness of traditional metal nitride bulk materials might be another fatal obstacle of their performance in pseudocapacitive application. By nanocrystallization and the surface partial oxidation, their irreformability of crystal structure declined, accompanied by the increase of the

vulnerability to electrolyte ions. And the drop of electro-conductibility due to nanometer effect[35] would be compensated by the recombination of high conductive RGO. Moreover in this graphene skeletonized architecture, the intergranular pores distributed around 6 - 8 nm and the interspaced pores among different RGO layers in range of 20 - 100 nm could guarantee the electrolyte ions to easily diffuse into the mesopores in the composites and effectively touch the surface of Ni_3N nanoparticles.[36] It was subsequently beneficial to the transfer of the electrolyte ions especially during the fast charge and discharge process, which was one of the key factors for electrochemical energy storage in high current and power density.

Electrochemical impedance spectroscopy (EIS) was used to further evaluate the performance of as-made Ni_3N/RGO electrode. As the confirmatory result was shown Fig. S7, at low frequencies in the Nyquist plot, a straight and nearly vertical line of Ni_3N/RGO electrode with a much bigger slope than pure Ni_3N exhibited, confirming the excellent capacitive behavior of the composites.[37] The Warburg region at medium frequencies, representative of the diffusion/transport of electrolyte ions, was short; indicating that the diffusion/transport of electrolyte ions was quite smooth due to the suitable mesoporosity in the RGO supported nanostructure.[37,38] Meanwhile, the reserved hydrophilic oxygen-containing functional group and doping N element in RGO improved the accessibility of electrolytes to

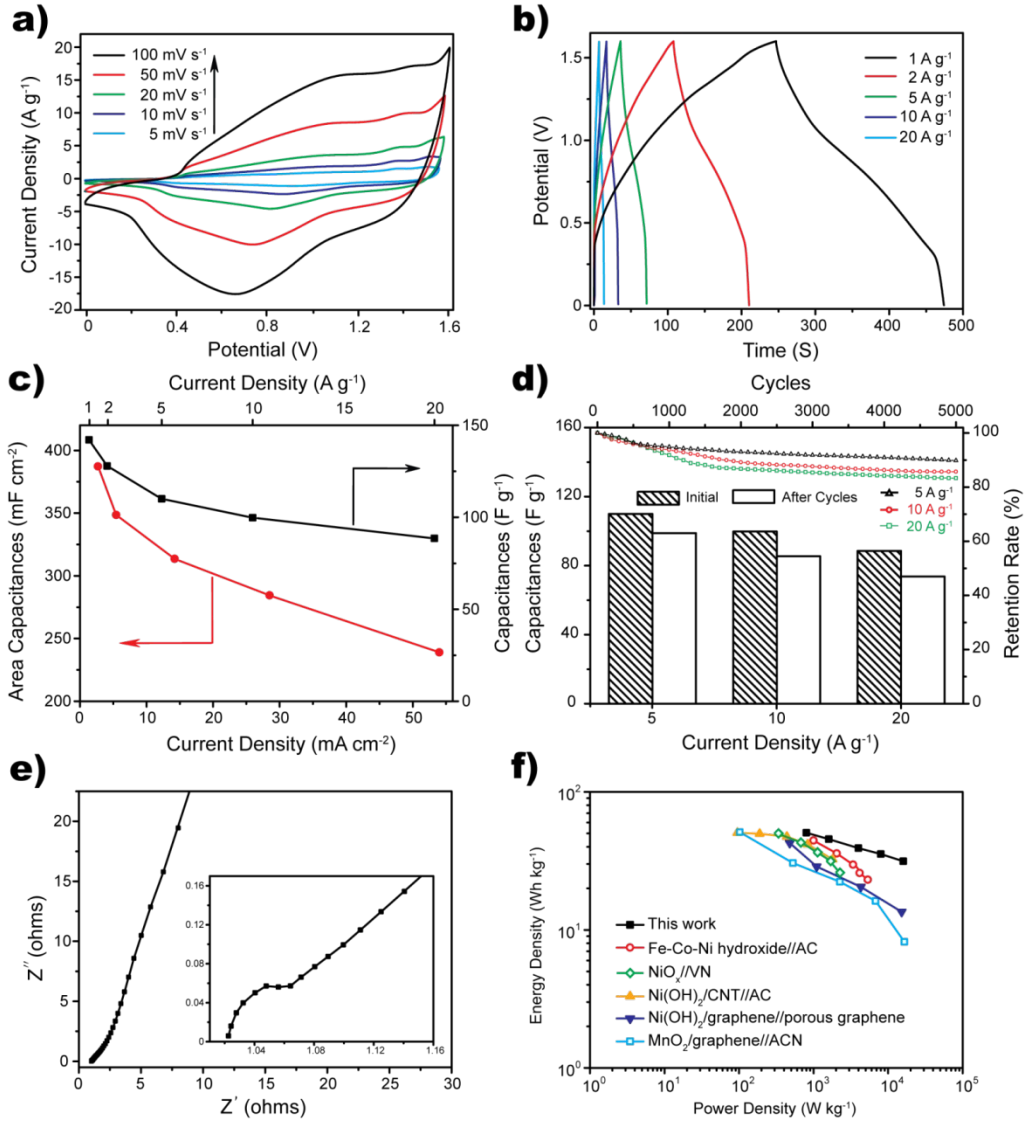

Fig. 5 (a) CV curves at various scan rates of 5 - 100 mV s^{-1} in a applied voltage window of 0 - 1.6 V, (b) galvanostatic charge/discharge voltage profiles at various current densities of 1 - 20 Ag^{-1} (based on the total mass of active materials from both electrodes), (c) the device and area capacitances calculated by galvanostatic charge/discharge voltage profiles, (d) Nyquist plots, (e) cycling stability at the 5, 10, and 20 A g^{-1}, (f) Ragone plots of the Ni_3N/RGO//DEG/RGO asymmetric supercapacitor; the histogram in the bottom of d) also shows the initial (stripy) and retained (blank) capacitances after cycles of asymmetric supercapacitor, and the inset of e is the magnifying EIS characterization in the high frequency region.

electrodes. A depressed and small semicircle was observed at high frequenciesin the amplifying Nyquist plot (as shown in inset of Fig. S7), and the equivalent series resistance (ESR) from the extrapolation ofthe vertical portion of the Nyquist plot to the real axis was estimated at 0.2Ω.

The cycling durability of Ni_3N/RGO was investigated at all the current densities. As shown in Fig. 4d, it had to be admitted that the specific capacitances of as-prepared composites declined at the early cycles, however, no sharp drops of C_s were presented after 2500 cycles. After 4000 cycles completing, more than 70 % retention of C_s still could be achieved. The capacitances at the end of 4000 cycling tests at 5 and 10 A g^{-1} reachedas high as 1310.9 and 1231.7 F g^{-1}, and also up to 791.7 F g^{-1} even at the fairly large current density as 100 A g^{-1}. With such high capacitance retention, the Ni_3N/RGO composites would be expected of an advantaged potential in application field.

Electrochemical Performance of the Ni_3N/RGO//DEG/RGO Asymmetric Supercapacitor

To further evaluate the Ni_3N/RGO electrode in the practical supercapacitor application, asymmetric supercapacitor cell was fabricated using Ni_3N/RGO and DEG/RGO[18] as the positive and negative electrodes, respectively (as shown in Fig. S8). CV measurements were performed to estimate the optimal voltage windows and mass ratio of the positive electrode to the negative electrode, also in 6 M KOH electrolyte. The voltage windows could be extended to 1.6 V, and the supercapacitors achieve the best with the ratio of Ni_3N/RGO to DEG/RGO as 0.34. CV curves at scan rates from 5 to 100 mV s^{-1} in Fig. 5a demonstrated the excellent capacitive behavior of as-fabricated asymmetric supercapacitor, which was mostly contributed by pseudo-capacitance of Ni_3N/RGO and electric double-layer capacitance of DEG/RGO. The amalgamative redox peaks of Ni_3N/RGO were much wider, with the anodic peak in the range of 0.4 - 1.2 V, while the cathodic peak from 1.0 - 0.2 V. There's no obvious anodic polarization curves representing irreversible O_2 evolution characteristics appearing, indicating the wide potentail window of 0 - 1.6 was reasonable.

Galvanostatic charge/discharge curves at different currentdensities of 1, 2, 5, 10, and 20 A g-1 (based on the total mass of activematerials from both positive and negative electrodes) are presented in Fig. 5b. It was obvious that the charge curve at 0 - 0.4 V and discharge curve at 0.3 - 0 V were approximately vertical, indicating the asymmetric supercapacitor possessed little capacitance in that voltage range. It was coincident with the CV information, and further confirmed the capacity of Ni_3N/RGO//DEG/RGO supercapacitor was based on the excellent pseudo-capacitance of positive electrode materials. The device capacitances of the asymmetric supercapacitor at different current densities were exhibited in Fig. 5c, as it reach a maximum of 142.1 F g^{-1}at 1 A g^{-1}. It is also necessary to calculate the area capacitance to evaluate the electrochemical performances of the asymmetric supercapacitor objectively. The area capacitances were in the range of 240 - 390 mF cm^{-2}, while the current densities were from about 3 to 55 mA cm^{-2}. Meanwhile, Ni_3N/RGO//DEG/RGO supercapacitor device reveals good rate capability. The device capacitance was up to 88.5 F g^{-1} even at a current density as high as 20 A g^{-1}, equivalent to 62.8 % of capacitance retention.

As shown in Fig. 5d, the cycling performance of the Ni_3N/RGO//DEG/RGO asymmetric supercapacitors was evaluated at the high current densities of 5, 10, and 20 A g^{-1}. At 5 A g^{-1}, the capacitance retains 89.8 % of its initial capacitance after 5000 cycles. Ever at 10 and 20 A g^{-1}, the capacitance loss were no more than 20 % (with retention ratio as 83.3 and 85.6 respectively). It should also benoted that, similar to the cycling performance in three-electrode system, the majority of capacitance loss happened in the initial 2000 cycles, and the capacitance retention of two-electrode asymmetric supercapacitors was superior to that in three-electrode system, which implied the compatibility of Ni_3N/RGO nanocomposites in the practical application. Moreover, the low resistance (about 1 Ω) of device reflected by Nyquist plots of asymmetric supercapacitors in Fig. 5e also signified the low energy loss during the massive charging and discharging processes. The Ragone plots of the asymmetric supercapacitors derived from the discharge curves are displayed in Fig. 5f. The highest energy density of supercapacitor can be calculated to be 50.5 Wh kg^{-1} at the average power density of 800.0 W kg^{-1} based on total mass of active materials, and still retained 31.5 Wh kg^{-1} even at high power density of 16.0kW kg^{-1}. These were advantageous over some recently reported nickel and manganese based asymmetric supercapacitors in aqueous electrolyte solutions, such as $Ni(OH)_2$/CNT//AC (32.5 Wh kg^{-1} at 1.8 kW kg^{-1}),[39] Fe-Co-Ni hydroxide//AC (23.9 Wh kg^{-1} at 5.36 kW kg^{-1}),[40] $Ni(OH)_2$/graphene//porous graphene (20.5 Wh kg^{-1} at 4.3 kW kg^{-1}),[41] and MnO_2/graphene//ACN (8.2 Wh kg^{-1} at 16.5kW kg^{-1}),[42] as well as the other nitride based system (NiO_x//VN, 26 Wh kg^{-1} at 2.4 kW kg^{-1}).[43]

Conclusions

In summary, a novel Ni_3N/RGO nanocomposite of small Ni_3N nanoparticles anchoring on the reduced graphene oxide nanosheets has been successfully synthesized, by the solvothermal treatment and following annealing under ammonia gas. The quite small size of Ni_3N crystals at about 10 nm endowed this composite excellent pseudo-supercapacitor performance, due to the remarkable increasing of the surface for faradic redox reaction, and the alleviation of the restrictions from volume change. Meanwhile, N doping and modification of ethylene glycol in the RGO sheets benefited the substrate texture with favorable hydrophilicity and good wettability with aqueous electrolyte. Also the hierarchical porosity among the nanoparticles and RGO layers facilitated the electrolyte ions to easily diffusion in the composites and effective contact with the pseudocapacitive materials. Mostly importantly, in contrast to the common Ni(II) compound, the Ni elements in Ni_3N experienced a two-step oxidation-reduction between Ni(I) and Ni(III) during the change/discharge processes, which could provided more faradic charge to equip the electrode material with more

pseudo-capacitance. The electrodes based on the as-obtained nanocomposite exhibited quite high specific capacitance at the ultrahigh current density (2087.5 F g^{-1} at 1 A g^{-1} and 1160.8 F g^{-1} at 100 A g^{-1}). This nanocomposite was also used to fabricate a Ni_3N/RGO//DEG/RGO asymmetric supercapacitor. The device delivered a high energy density of 50.5 Wh kg^{-1} at a power density of 800 W kg^{-1}, and even maintain above 30 Wh kg^{-1} at 16.0 kW kg^{-1}, while its capacitance retentions exceeded 80% after 5000 cycles at different high device current densities. Consequently, this kind of Ni_3N/RGO nanocomposite could be seemed as a competitive and qualified candidate for energy storage, and such a method might extend the strategy for preparing nanostructured supercapacitor electrode materials.

Acknowledgements

We gratefully thank the financial support by the Fundamental Research Funds for the Central Universities of China (2015JBM102, S13JB00200), Beijing Jiaotong University and the Ministry of Education of China (2014RC026), China Postdoctoral Science Foundation (2015M570922), National Natural Science Foundation of China (NSFC11079010), and the Key Laboratory of Carbon Materials (KLCMKFJJ1401).

Notes and references

1. P. Simon and Y. Gogotsi, *Nat. Mater.*, 2008, **7**, 845-854.
2. J. Yan, Q. Wang, T. Wei and Z. Fan, *Adv. Energy Mater.*, DOI: 10.1002/aenm.201300816.
3. L. L. Zhang, R. Zhou and X. S. Zhao, *J. Mater. Chem.*, 2010, **20**, 5983-5992.
4. K. S. Novoselov, A. K. Geim, S. Morozov, D. Jiang, Y. Zhang, S. Dubonos, I. Grigorieva and A. Firsov, *science*, 2004, **306**, 666-669.
5. K.-W. Nam and K.-B. Kim, *J. Electrochem. Soc.*, 2002, **149**, A346-A354.
6. M. P. Yeager, D. Su, N. S. Marinković and X. Teng, *J. Electrochem. Soc.*, 2012, **159**, A1598-A1603.
7. D. Su, H.-S. Kim, W.-S. Kim and G. Wang, *Chem. Eur. J.*, 2012, **18**, 8224-8229.
8. X. Zhang, W. Shi, J. Zhu, W. Zhao, J. Ma, S. Mhaisalkar, T. Maria, Y. Yang, H. Zhang, H. Hng and Q. Yan, *Nano Res.*, 2010, **3**, 643-652.
9. C. Yuan, X. Zhang, L. Su, B. Gao and L. Shen, *J. Mater. Chem.*, 2009, **19**, 5772-5777.
10. J. Y. Lee, K. Liang, K. H. An and Y. H. Lee, *Synthetic Met.*, 2005, **150**, 153-157.
11. B. Zhao, J. Song, P. Liu, W. Xu, T. Fang, Z. Jiao, H. Zhang and Y. Jiang, *J. Mater. Chem.*, 2011, **21**, 18792-18798.
12. H. Wang, H. S. Casalongue, Y. Liang and H. Dai, *J. Am. Chem. Soc.*, 2010, **132**, 7472-7477.
13. S. Dong, X. Chen, X. Zhang and G. Cui, *Coord. Chem. Rev.*, 2013, **257**, 1946-1956.
14. S. Bouhtiyya, R. Lucio-Porto, J.-B. Ducros, P. Boulet, F. Capon, T. Brousse and J.-F. Pierson, *Honolulu Prime*, 2012, Abstract #494.
15. F. Gillot, J. Oro-Sole and M. R. Palacin, *J. Mater. Chem.*, 2011, **21**, 9997-10002.
16. X. Li, M. M. Hasan, A. L. Hector and J. R. Owen, *J. Mater. Chem. A*, 2013, **1**, 6441-6445.
17. D. C. Marcano, D. V. Kosynkin, J. M. Berlin, A. Sinitskii, Z. Sun, A. Slesarev, L. B. Alemany, W. Lu and J. M. Tour, *ACS Nano*, 2010, **4**, 4806-4814.
18. Y. Yu, Y. Sun, C. Cao, S. Yang, H. Liu, P. Li, P. Huang and W. Song, *J. Mater. Chem. A*, 2014, **2**, 7706-7710.
19. N. S. Gajbhiye, R. S. Ningthoujam and J. Weissmüller, *phys. status solidi A*, 2002, **189**, 691-695.
20. D. Chen and X. Jiao, *J. Am. Ceram. Soc.*, 2000, **83**, 2637-2639.
21. F. Tuinstra and J. L. Koenig, *J. Chem. Phys.*, 1970, **53**, 1126-1130.
22. S. Stankovich, D. A. Dikin, R. D. Piner, K. A. Kohlhaas, A. Kleinhammes, Y. Jia, Y. Wu, S. T. Nguyen and R. S. Ruoff, *Carbon*, 2007, **45**, 1558-1565.
23. C. Zhang, L. Fu, N. Liu, M. Liu, Y. Wang and Z. Liu, *Adv. Mater.*, 2011, **23**, 1020-1024.
24. Y. Wang, Z.-W. Fu, X.-L. Yue and Q.-Z. Qin, *J. Electrochem. Soc.*, 2004, **151**, E162-E167.
25. R. Dhunna, C. Lal, D. K. Avasthi, S. R. Barman, V. Ganesan and I. P. Jain, *Vacuum*, 2009, **83**, 1448-1453.
26. G. Ertl, R. Hierl, H. Knözinger, N. Thiele and H. P. Urbach, *Appl. Surf. Sci.*, 1980, **5**, 49-64.
27. D. Choi, G. E. Blomgren and P. N. Kumta, *Adv. Mater.*, 2006, **18**, 1178-1182.
28. L. Qu, Y. Liu, J.-B. Baek and L. Dai, *ACS Nano*, 2010, **4**, 1321-1326.
29. D. Wei, Y. Liu, Y. Wang, H. Zhang, L. Huang and G. Yu, *Nano Lett.*, 2009, **9**, 1752-1758.
30. D. T. Clark and H. R. Thomas, *J Polym. Sci. Pol. Chem.*, 1978, **16**, 791-820.
31. T. Y. Kim, H. W. Lee, M. Stoller, D. R. Dreyer, C. W. Bielawski, R. S. Ruoff and K. S. Suh, *ACS Nano*, 2010, **5**, 436-442.
32. Z. Lin, Y. Liu, Y. Yao, O. J. Hildreth, Z. Li, K. Moon and C.-p. Wong, *J. Phys. Chem. C*, 2011, **115**, 7120-7125.
33. X. Lu, G. Wang, T. Zhai, M. Yu, S. Xie, Y. Ling, C. Liang, Y. Tong and Y. Li, *Nano Lett.*, 2012, **12**, 5376-5381.
34. X. Lu, T. Liu, T. Zhai, G. Wang, M. Yu, S. Xie, Y. Ling, C. Liang, Y. Tong and Y. Li, *Adv. Energy Mater.*, DOI: 10.1002/aenm.201300994.
35. K. Xu, P. Chen, X. Li, Y. Tong, H. Ding, X. Wu, W. Chu, Z. Peng, C. Wu and Y. Xie, *J. Am. Chem. Soc.*, 2015, **137**, 4119.
36. S. Peng, L. Li, H. B. Wu, S. Madhavi and X. W. Lou, *Adv. Energy Mater.*, DOI: 10.1002/aenm.201401172.
37. Y. Li, Z. Li and P. K. Shen, *Adv. Mater.*, 2013, **25**, 2474-2480.
38. K. Zhang, L. L. Zhang, X. S. Zhao and J. Wu, *Chem. Mater.*, 2010, **22**, 1392-1401.
39. Z. Tang, C.-h. Tang and H. Gong, *Adv. Funct. Mater.*, 2012, **22**, 1272-1278.
40. H. Li, Y. Gao, C. Wang and G. Yang, *Adv. Energy Mater.*, DOI: 10.1002/aenm.201401767.
41. J. Yan, Z. Fan, W. Sun, G. Ning, T. Wei, Q. Zhang, R. Zhang, L. Zhi and F. Wei, *Adv. Funct. Mater.*, 2012, **22**, 2632-2641.
42. Z. Fan, J. Yan, T. Wei, L. Zhi, G. Ning, T. Li and F. Wei, *Adv. Funct. Mater.*, 2011, **21**, 2366-2375.
43. Z. Gao, H. Zhang, G. Cao, M. Han and Y. Yang, *Electrochim. Acta*, 2013, **87**, 375-380.

Broader Context:

A novel Ni_3N/Graphene nanocomposite has been synthesized as pseudo supercapacitors electrode material with high capacitance and energy density, due to its unique two-step oxidation/reduction reaction mechanism.

TOC Graphic and text:

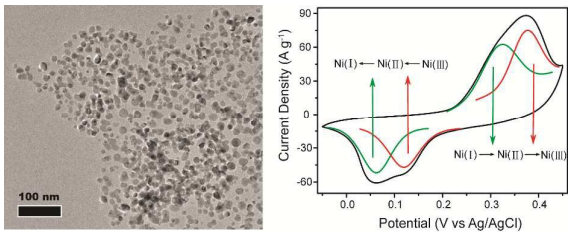

A Novel Ni_3N/Graphene Nanocomposite as Supercapacitor Electrode Material with High Capacitance and Energy Density